ISSN 1541-308X, Physics of Wave Phenomena, 2018, Vol. 26, No. 3, pp. 221–233. © Allerton Press, Inc., 2018.

DYNAMICS OF LIQUID CLUSTERS IN AN ELECTRICAL FIELD

Damping Oscillations of Microdroplets of a Droplet Cluster in an External Electric Field

D. N. Gabyshev*

Tyumen State University, ul. Volodarsky 6, Tyumen, 625003 Russia

Received May 15, 2018

Abstract—The forces acting on levitating water microdroplets in the structure of a droplet cluster (A.A. Fedorets, 2004) have been analyzed. It is found that microdroplets in the cluster should undergo low-frequency vertical damping oscillations near the equilibrium position. Oscillations occur also when switching on an external electric field, which affects the oscillation frequency and equilibrium position. Microdroplets are shown to lose their stability in the critical range of parameters. The electric fields are calculated in the simplest experimental scheme for simulating the effect of electric field on a droplet cluster.

DOI: 10.3103/S1541308X1803007X

1. INTRODUCTION

An observation of mist above heated water surface reveals the existence of microscopic droplets in it, which are suspended due to the equilibrium between the pressure force of ascending vapor-air flow and the gravity force [1]. It has also been noted that suspended droplets disappear when bringing an electrified ebonite stick to them, a fact suggesting that microdroplets are electrically charged.

Suspended microdroplets can form an ordered structure (droplet cluster) [2], where water microdroplets arise above a locally heated submillimeter water layer to form a hexagonally ordered monolayer. The characteristic size of microdroplets and their height above the water layer are several tens of micrometers. The droplet cluster turned out to be a convenient tool for observing liquid microdroplets on the minute scale. Grounding of a cuvette with water in the first experiments did not visibly affect the cluster stability; therefore, it was concluded that noncoalescence of microdroplets inside a droplet cluster is not attributable to the electrostatic charging [3].

The direct effect of electric field on a droplet cluster was experimentally studied in detail in [4] (later on, the cluster was investigated in an IR electromagnetic field [5, 6]). In the experiment performed in [4], a vertical 0.16-mm-thick electrode was located above the droplet cluster, and the plane water surface served as the other electrode. The interelectrode distance was 3 to 5 mm, and the maximum potential difference was 1.5 kV. All the effects were explained in [4] proceeding from the plasma-dust analogy, when field inhomogeneity and microdroplet polarization neglected. At the same time, according to the estimation of [7], the error in determining the field strength reached $\pm 50\%$, which should affect the accuracy of estimating the positive charge of microdroplets ($10^3|e|$, where e is the elementary charge). It was admitted that the charge cannot determine to a great extent the levitation according to the Coulomb levitation mechanism, and it is the Stokes levitation mechanism that is decisive [4].

The plasma-dust interpretation of a droplet cluster was disputed in [8]. In addition, several models were proposed, which do not consider necessary the presence of initial electric charge on water droplets to explain their behavior in an electrostatic field [9] (see also [10]). Thus, the origin of the charge of water microdroplets in a cluster appears to be debated. This is an important question, if only because the intrinsic charge of microdroplets should affect the kinetics of their condensation growth [11]. In addition, the possibility of controlling water microvolumes using dielectrophoresis (by analogy with nanopipettes) may be promising [12].

The purpose of our study was to develop a physical model of the levitation of a microdroplet from a droplet cluster in an external field, with allowance for both the charge and polarization of this microdroplet. The study includes an analytical calculation aimed at estimating the electric fields in the cluster region (applying a possible experimental scheme) and a calculation of the mechanical motion of microdroplets in the estimated electric field.

*E-mail: gabyshev-dmitrij@rambler.ru

2. SUGGESTION OF A POSSIBLE EXPERIMENTAL SCHEME

Let ε_{sub} be the permittivity of a flat round substrate (disk) with radius a and thickness δ_{sub} (Fig. 1). There is a submillimeter water layer with thickness δ and permittivity ε on the substrate surface. Let there be a thin conducting layer of thickness δ_{con} between the substrate and water, which uniformly covers the substrate. This layer serves as one of the electrodes. The other electrode is a thin straight-line wire with diameter d and length $2L$, located normally to the substrate along its axis. The interelectrode distance D is considered to be the shortest distance from the lower tip of the upper electrode to the lower disk electrode.

Let the semitransparent substrate be locally heated at the center (for example, by a laser beam, as in [5, 6]). The water layer is slowly evaporated in the heated region, and, as a result of condensation, microdroplets are formed above it; they levitate at a height H on the order of their intrinsic diameter $2R$. These microdroplets form a droplet cluster [2], whose maximum size is related to the size of the heated region and does not exceed 1 mm. Microdroplets are located mainly in the same plane (two-dimensional aerosol).

For simplicity, it is convenient to apply an electric potential (positive for definiteness) to only one electrode and keep the other electrode grounded. The metal elements of real system housing should to be separated by a sufficiently large distance to exclude the effect of mirror charges on the statement of experiment. The problem of the behavior of microdroplets in a droplet cluster is reduced to calculation of the electric field in which these microdroplets exist. Below we perform a fairly rough analytical calculation, which, however, takes into account the field inhomogeneity and, therefore, is more exact than the estimation of [4].

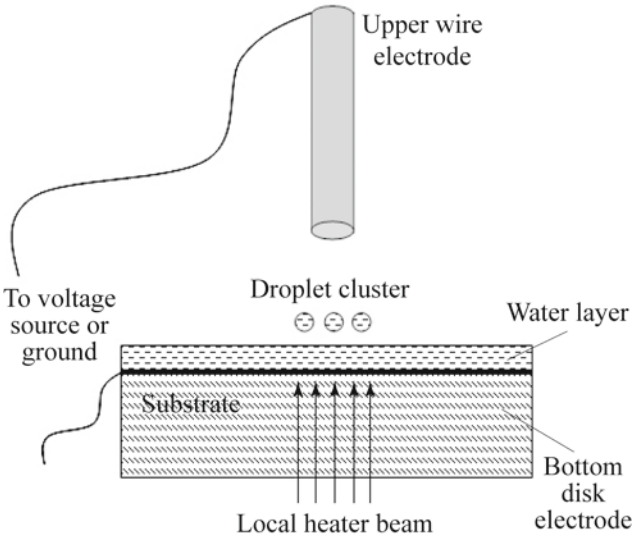

Fig. 1. Relative position of electrodes and a droplet cluster.

3. CALCULATION OF ELECTRIC FIELDS

3.1. Analytical Calculation

Let us assume that a positive potential $\varphi_0 > 0$ is applied to the upper electrode (see Fig. 1) and charges are distributed uniformly over its surface. We denote the potential formed in space by φ_0 as $\varphi_u(r, s, \sigma_{u|\varphi})$, where s is the length of the perpendicular from the point in space under consideration to the electrode axis, r is the distance from the electrode end to this perpendicular, and parameter $\sigma_{u|\varphi}$ is the surface charge density on the upper electrode. The potential φ_u can be found from the Gauss theorem (see Appendix). The droplet cluster is concentrated almost on the axis of the upper electrode; hence, the displacement s for it is always close to zero.

The lower grounded electrode in the field of the upper electrode acquires a negative charge. On the assumption of uniform distribution of induced charges over the electrode surface, their density can be estimated as

$$\sigma_{b|\text{ind}} \approx -\frac{\varphi_u(D, 0, \sigma_{u|\varphi})\, C_b}{\pi a^2}, \qquad (1)$$

where C_b is the lower electrode capacitance (which is approximately the same as for a flattened ellipsoid [13]). The estimate given by (1) somewhat exceeds the true averaged value because of the large distance between the disk edges and upper electrode. Therefore, the analytical calculation performed below is in essence one-dimensional: we use the value of surface charge density (1) on the axis instead of the exact variable value, implying the parameters of spatial objects (capacitance and displacement from the axis, s). In addition, the denominator in the expression for $\sigma_{b|\text{ind}}$ is valid for only a very thin disk ($\delta_{\text{con}} \gg a$), so that the charges on the upper and lower surfaces of the disk electrode are assumed to be identical. This approximation is acceptable for electrodes of submicron thickness, formed by depositing a conducting material on a substrate.

A disk with induced charges forms an intrinsic field $\varphi_b(D - r, s, \sigma_{b|\text{ind}})$ in the space above it. With the water and substrate disregarded, the potential in the interelectrode gap is equal to the sum $\varphi_u(r, s, \sigma_{u|\text{ind}}) + \varphi_b(D - r, s, \sigma_{b|\text{ind}})$. The strength E_{ex}, as the gradient of this potential with a minus sign, polarizes both the water layer and the substrate. The dipole moment of a round water layer (polar

dielectric) of radius a and thickness δ, with a permittivity ε, can be calculated using the Langevin–Debye relation

$$\wp_w = 3\pi\varepsilon_0 a^2\delta\,\frac{\varepsilon-1}{\varepsilon+2}E_{\text{ex}}. \quad (2)$$

The dipole moment of a disk substrate (isotropic dielectric) is calculated by definition

$$\wp_{\text{sub}} = \varepsilon_0\kappa E_{\text{ex}}\pi a^2\delta_{\text{sub}}, \quad (3)$$

where $\kappa=\varepsilon_{\text{sub}}-1$ is the dielectric susceptibility of the substrate material. When calculating the polarization, we will take its value only on the axis (as previously for the charge density). The field component $E_{\text{ex}\perp}$ oriented perpendicular to the axis of the system is small and varies only slightly when moving away from the axis. Therefore, we can simplify the calculation by neglecting this component $E_{\text{ex}\perp}$ and taking into account only the component $E_{\text{ex}\parallel}$ oriented parallel to the axis of the entire system. The strength drop across the water layer (less than 1 mm thick) is rather large; therefore, bound charges with different moduli are formed on the upper and lower layer surfaces; the densities of these charges are given by the formula

$$\sigma_{w|\text{pol}} = \frac{\wp_w}{\pi a^2\delta}, \quad (4)$$

in which the external field $E_{\text{ex}\parallel}$ must be taken, respectively, on the upper and lower water surfaces. This circumstance will be reflected through subscripts "ab" and "be" (above and below, respectively). The bound charges on the substrate are calculated and denoted similarly. The bound water charges are dispersed over round surfaces; hence, to calculate the field formed by these charges in space, one can use the function φ_b, having substituted necessary arguments.

In total, the electric field in the region of droplet cluster is the sum of four fields, formed by the upper wire electrode with a surface charge density $\sigma=\sigma_{u|\varphi}$; free water plane ($\sigma=-\sigma_{w|\text{pol}|\text{ab}}$); lower electrode ($\sigma=\sigma_{b|\text{ind}}+\sigma_{w|\text{pol}|\text{be}}-\sigma_{\text{sub}|\text{pol}|\text{ab}}$); and, finally, the lower plane of the dielectric substrate ($\sigma=\sigma_{\text{sub}|\text{pol}|\text{be}}$). The potential and strength at the point spaced by a distance η from the water surface and located near the axis of the system ($s\ll a$) can be written as

$$\begin{aligned}\Phi(\eta,s) &= \varphi_u(D-\delta-\eta,s,\sigma_{u|\varphi})\\ &+\varphi_b(\eta,s,-\sigma_{w|\text{pol}|\text{ab}})\\ &+\varphi_b(\delta+\eta,s,\sigma_{b|\text{ind}}+\sigma_{w|\text{pol}|\text{be}}-\sigma_{\text{sub}|\text{pol}|\text{ab}})\\ &+\varphi_b(\delta_{\text{sub}}+\delta_{\text{con}}+\delta+\eta,s,\sigma_{\text{sub}|\text{pol}|\text{be}}), \quad (5)\\ E_{\parallel}(\eta,s) &= -\frac{\partial}{\partial\eta}\,\Phi(\eta,s)\end{aligned}$$

(see Appendix).

This analytical scheme is quite applicable for the case where potential φ_0 is applied to the lower electrode, whereas the upper electrode is grounded. Then the field in the droplet cluster region is also the sum of four fields: from the lower disk electrode ($\sigma=\sigma_{b|\varphi}+\sigma_{w|\text{pol}|\text{be}}-\sigma_{\text{sub}|\text{pol}|\text{ab}}$), free water surface ($\sigma=-\sigma_{w|\text{pol}|\text{ab}}$), lower substrate surface ($\sigma=\sigma_{\text{sub}|\text{pol}|\text{be}}$), and upper wire electrode ($\sigma=\sigma_{u|\text{ind}}$). The field formed by the grounded electrode can often be neglected in applied calculations.

3.2. Results of Numerical Calculation

The realistic values of physical and geometric parameters of the system will be taken for computer calculations as follows: the upper vertical electrode length $2L=2\times10^{-2}$ m, the upper electrode diameter $d=200\times10^{-6}$ m, the water layer thickness $\delta=500\times10^{-6}$ m, the radius of the substrate and lower electrode $a=10^{-2}$ m, the lower electrode thickness $\delta_{\text{ox}}=500\times10^{-9}$ m, the substrate thickness $\delta_{\text{sub}}=2\times10^{-3}$ m, the microdroplet levitation height above the water surface $H=100\times10^{-6}$ m, the microdroplet displacement from the axis of the system $s=0$ m, the water permittivity $\varepsilon=57$ (at 92.8°C), and the substrate material permittivity $\varepsilon_{\text{sub}}=3.75$ (corresponds to quartz glass).

Let a potential be applied to the upper electrode. A calculation (Figs. 2–5) shows that the strength E decreases in modulus when moving away from the upper electrode (i.e., when the distance to water η decreases). However, near the lower electrode, it, on the contrary, begins to rise because of the negative induction charges, leaking into the lower grounded electrode. At the point where the strength stops decreasing and starts increasing, the derivative of the vertical component E is zero (see Figs. 3 and 5). The position of the extreme point depends strongly on the interelectrode distance D, but is independent of potential φ_0 in view of the linear dependence of $\Phi(\eta,s)$ on this potential. The extreme point divides the field into two regions (see Figs. 3 and 5). In region I, the upper electrode with active potential φ_0 plays a key role. In region II, the field is mainly induced by the charges on the lower electrode.

When the interelectrode distance D is large (>1 cm, case of high electrode), region II is also large and covers a quarter of interelectrode gap (see Fig. 3). When the upper electrode is located at a small distance ($D\approx1$ cm or smaller, low electrode), region II is much smaller, and the distance to the extreme point is now on the submillimeter scale (see Fig. 5). With a further decrease in D for a low electrode, the extreme point, according to the analytical calculations (Subsec. 3.1), may even pass into the water layer;

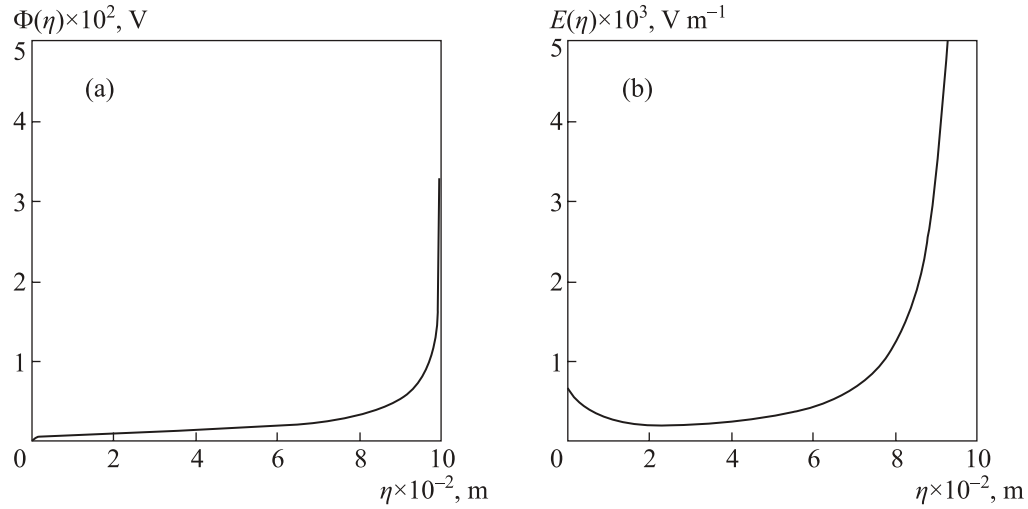

Fig. 2. Potential Φ (a) and strength E (b) of electric field in the interelectrode gap on the axis of the system ($s = 0$) in dependence on the distance η to the water layer at $\varphi_0 = 500$ V and interelectrode distance $D = 10$ cm (high electrode).

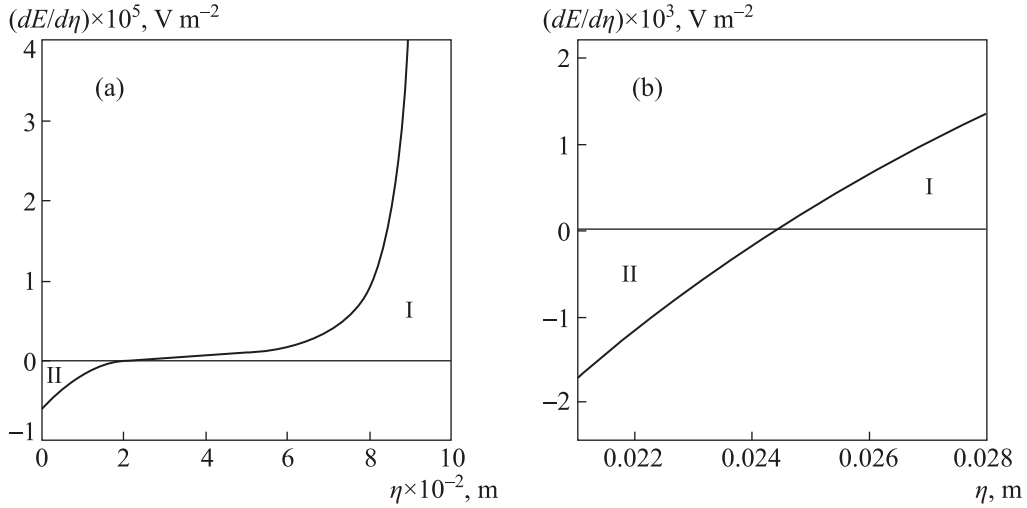

Fig. 3. Derivative (a) of the vertical component of the electric field strength on the axis of the system ($s = 0$) and an enlarged fragment near the intersection with zero (b), in dependence on the distance η to the water layer at $\varphi_0 = 500$ V and $D = 10$ cm (high electrode).

however, the calculation should be slightly corrected in this case, because the polarity of free water surface changes. In addition, when the extreme point is close to the water layer, quantitative results are determined to a great extent by the assumptions and simplifications used to calculate field in Subsec. 3.1. It is of key importance that a decrease in D diminishes the sizes of region II to submillimeter scale. For example, at $D = 9.2\times10^{-3}$ m, the inflection point is located at a height of 56 μm, which is smaller than the levitation height H accepted in the model. This circumstance is interesting for the following reason: the dielectrophoretic force acting on microdroplets is directed upwards in this case. This force configuration is considered below (see Subsec. 4.3). If a potential φ_0 is applied to the lower electrode, and the upper electrode is grounded, the fields are similar to those depicted in Figs. 2 and 3, but region II is much larger. In Sec. 4, the calculated fields are used as a base for developing a model of mechanical motion of microdroplets in electric field.

4. DROPLET LEVITATION

4.1. Free Droplet Levitation

The experiments performed in [2–7] showed that microdroplets are retained above the water layer at an almost constant height. The second Newton law for microdroplets in the absence of electric field can be written as

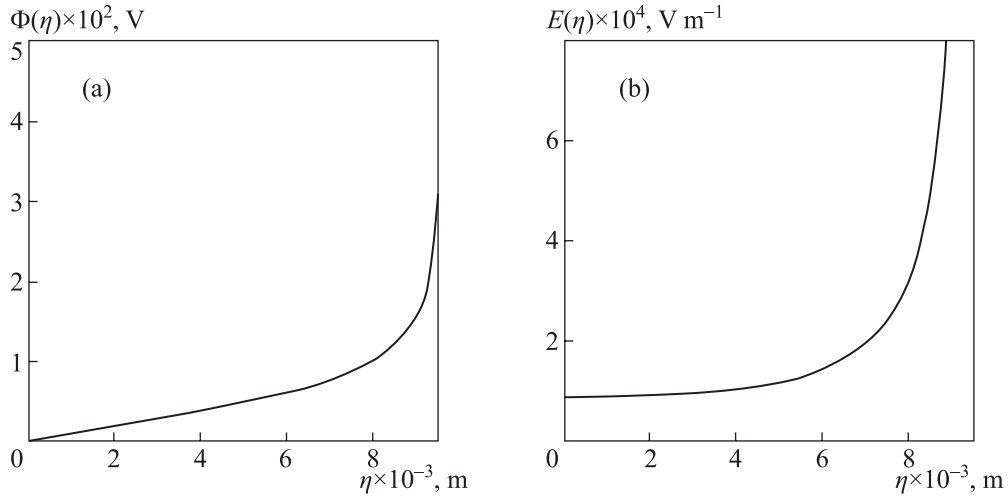

Fig. 4. Potential (a) and strength (b) of the electric field in the interelectrode gap on the axis of the system ($s = 0$) in dependence on the distance η to the water layer at $\varphi_0 = 500$ V and interelectrode distance $D = 1$ cm (low electrode).

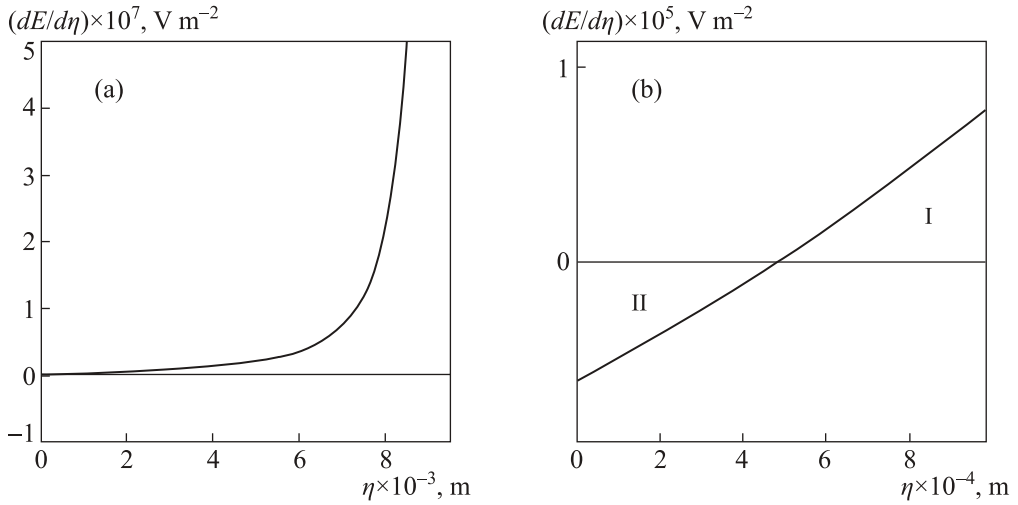

Fig. 5. Derivative (a) of the vertical component of electric field strength on the axis of the system ($s = 0$) and an enlarged fragment near the intersection with zero (b), in dependence on the distance η to the water layer at $\varphi_0 = 500$ V and $D = 1$ cm (low electrode).

$$\mathbf{F} = m\mathbf{g} + \mathbf{F}_d + \mathbf{F}_\mathrm{A}, \tag{6}$$

where $m\mathbf{g}$ is the gravity force for a droplet, $\mathbf{F}_d$ is the force from the side of ascending vapor-air flow, $\mathbf{F}_\mathrm{A}$ is the buoyancy force, and $\mathbf{F}$ is the resulting force. We choose a frame of reference where a droplet is on average at rest (Fig. 6) and the **x** axis is directed upwards. The second Newton law in projection on the **x** axis has the form

$$F = -mg + F_d + F_\mathrm{A}. \tag{7}$$

The gravity force for a spherical microdroplets is

$$mg = \frac{4}{3}\pi R^3 \rho_w g, \tag{8}$$

where the water density $\rho_w = 963.4\,\mathrm{kg\,m^{-3}}$ (at 92.8°C). The buoyancy force for a sphere moving

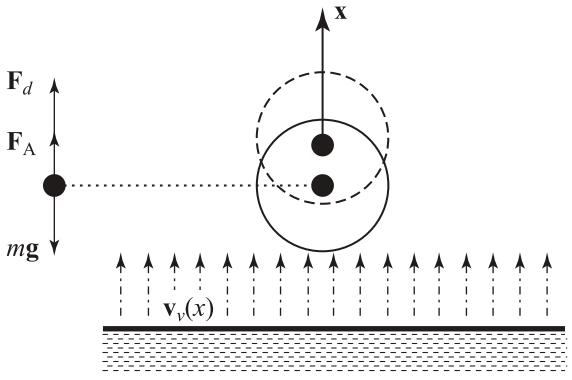

Fig. 6. Droplet in ascending steam-air flow.

with acceleration in an ascending flow of density $\rho_v \approx 1.01\,\mathrm{kg\,m^{-3}}$ [14] is

$$F_\mathrm{A} = \frac{4}{3}\pi R^3 \rho_v \left(g - \frac{\ddot{x}}{2}\right). \tag{9}$$

The force exerted by the ascending flow in the simplest form is taken to be equal to the Stokes force [15, 16]:

$$F_{d0} = 6\pi R\mu\, v_r, \tag{10}$$

where $\mu = 2\times10^{-5}\,\mathrm{kg\,m^{-1}\,s^{-1}}$ is the dynamic viscosity of the vapor-air mixture. Here, the flow velocity v_v and the intrinsic droplet velocity $\dot{x}$ are taken into account in the droplet velocity with respect to the flow: $v_r = v_v - \dot{x}$. The velocity distribution in the flow, $v_v = v_v(x)$, is almost stationary, but depends on temperature in the heated region (see Fig. 1). Near the origin of coordinates, it can be written as

$$v_v \approx (1 + kx)v, \tag{11}$$

where v is the velocity at $x = 0$ and $k = (1/v) \times (dv_v/dx)|_{x=0} < 0$ (the flow is similar to the so-called submerged jet [17]). According to [18], the gradient kv is independent (within the experimental accuracy) of the temperature of the water interface and ranges from -0.2×10^3 to $-1.0\times10^3\,\mathrm{s^{-1}}$. We will use the mean value from this interval.

Thus, the ordinary Stokes force is approximately equal to

$$F_{d0} = 6\pi R\mu\big[v(1 + kx) - \dot{x}\big]. \tag{12}$$

Note also that this formula was corrected in [4] as applied to a droplet cluster, with allowance for the fact that the aerodynamic force increases when a microdroplet approaches the water surface (due to the air-cushion effect). However, despite that fact that the approximation of [4] describes qualitatively the pattern for a thin gap between the droplet and water surface, it is inconsistent with real experiments because yields an infinite force when the gap tends to zero. In reality, the droplet should coalesce with the water surface. This drawback can be eliminated by introducing three independent correction coefficients α_1, α_2, and α_3 into the formula from [4]:

$$F_d = F_{d0}\alpha_1\left(1 + \frac{\alpha_2 R}{H - R + x + \alpha_3}\right). \tag{13}$$

In the model considered in [4], these coefficients are taken to be $\alpha_1 = 1$, $\alpha_2 = 1$, and $\alpha_3 = 0$. They can be refined based on known experimental data. For a temperature of 92.8°C, these coefficients, found by the least-squares method from the plots reported in [18], are as follows (with a correlation coefficient of 0.9811):

$$\begin{aligned} &\alpha_1 = \frac{2g(\rho_\mathrm{w} - \rho_v)}{9\mu v A_1},\\ &\alpha_2 = 1.061, \quad \alpha_3 = 5.568\times10^{-6}\,\mathrm{m},\\ &A_1 = 1.433\times10^9\,\mathrm{m^{-2}}. \end{aligned} \tag{14}$$

The way to calculate these coefficients will be briefly described in Subsec. 4.3.

Thus, we now know all the forces keeping a microdroplet in vertical equilibrium.

4.2. Electrokinetic Forces Acting on Microdroplets

Let an external electrostatic field be instantaneously switched on. An electrokinetic (EK) force arises in its presence, which is equal to the sum of electrophoretic (EP) and dielectrophoretic (DP) forces [19, 20]:

$$\mathbf{F}_\mathrm{EK} = q\mathbf{E} + \sum_n (p^{(n)}\cdot\nabla^n)\,\mathbf{E},$$

where $\mathbf{p}^{(n)}$ are nth-order multipole moments and q is the microdroplet charge. The EP force for positive and negative charges is directed, respectively, along and opposite the field force lines. The DP force is always directed towards the force line concentration (where the field strength increases in modulus), and this is specifically the force that, e.g., makes small scraps of paper stick to an ebonite rod rubbed with wool. From the applied point of view, this force is of interest for controlling micro- and nano-objects [12].

In most problems, it is sufficient to restrict oneself to the first multipole approximation. The dipole moment of water microdroplets can be obtained (either from [13] or from the Langevin–Debye relation) in the form

$$\wp_b = 4\pi\varepsilon_0 \frac{\varepsilon - 1}{\varepsilon + 2} R^3 \mathbf{E}_\mathrm{ex}. \tag{15}$$

Let the field near zero change only slightly and be almost linear:

$$E(x) \approx E_0(1 + \lambda x), \tag{16}$$

where E_0 is the electric field strength at $x = 0$, $\lambda = (1/E_0)(dE/dx)|_{x=0}$. Then the electrokinetic force component along the x axis is

$$\begin{aligned} F_\mathrm{EK} &= F_\mathrm{EP} + F_\mathrm{DP} = qE_\mathrm{ex} + \wp_b \frac{dE_\mathrm{ex}}{dx}\\ &= \left(q + 4\pi\varepsilon_0 \frac{\varepsilon - 1}{\varepsilon + 2} R^3 \frac{dE}{dx}\right) E(x), \end{aligned} \tag{17}$$

where $q > 0$ (for definiteness), $E_0 < 0$, $dE/dx < 0$, and $\lambda > 0$; the field is directed downwards, and the field force lines concentrated to the top (as in Subsec. 3.2), whereas the DP force is directed upwards,

which correspond to region I in Fig. 5 (in region II this force is directed downwards to water). The x axis in Fig. 6 and the η axis in Figs. 2 and 4 are antiparallel; therefore, the strength values from Figs. 2 and 4 should be taken for calculations with a minus sign. We assume for simplicity that the characteristic sizes of field inhomogeneity exceed the microdroplet sizes. The possible presence of a relatively low intrinsic charge q on microdroplets and the formation of an ordered cluster by these droplets are not contradictory: it is well known that the Coulomb law for charged spheres is significantly corrected at small distances, up to the transition from repulsion to attraction [21–24].

4.3. Derivation of the Equation of Motion

The second Newton law for a microdroplet in an electrostatic field can be written as

$$\mathbf{F} = m\mathbf{g} + \mathbf{F}_d + \mathbf{F}_{\rm A} + \mathbf{F}_{\rm EK}. \tag{18}$$

Let the electrokinetic force be directed upwards; then, the component of the force (18) along the **x** axis is

$$F = -mg + F_d + F_{\rm A} + F_{\rm EK}, \tag{19}$$

and the equation of motion for a microdroplet has the form

$$\frac{4}{3}\pi R^3\rho_w\ddot{x} = -\frac{4}{3}\pi R^3\rho_w g + 6\pi R\mu\Big[v(1+kx) - \dot{x}\Big]\alpha_1\left(1 + \frac{\alpha_2 R}{H - R + x + \alpha_3}\right)$$
$$+ \frac{4}{3}\pi R^3\rho_v\left(g - \frac{\ddot{x}}{2}\right) + qE_0(1+\lambda x) + 4\pi\varepsilon_0\frac{\varepsilon-1}{\varepsilon+2}R^3\frac{dE}{dx}E_0(1+\lambda x). \tag{20}$$

Experimental relations between radius R and levitation height H (see Fig. 2 in [18]) occur both in the absence of field and in equilibrium ($x=0$, $\dot{x}=0$, and $\ddot{x}=0$). Based on the dependence $H(R)$ and formula (20), one can find coefficients α_1, α_2, and α_3 by the least-squares method; the calculated values were presented in Subsec. 4.1. Using these coefficients, one can put an equilibrium radius R into correspondence with each height H by solving the cubic equation with respect to R, which stems from (20). For example, at $H = 100\,\mu$m, we have approximately $R = 32\,\mu$m.

Let us transform Eq. (20) by introducing the following definitions:

$$K \stackrel{\rm def}{=} \frac{1}{\rho_w + \rho_v/2}\frac{9\mu\alpha_1}{2R^2} = \frac{g}{vA_1R^2}\frac{\rho_w - \rho_v}{\rho_w + \rho_v/2}, \quad \widetilde{h} \stackrel{\rm def}{=} H - R + \alpha_3. \tag{21}$$

In the linear approximation, $(dE/dx)|_x = (dE/dx)|_{x=0}$ and, therefore, $(1/E_0)(dE/dx)|_x = \lambda$. After introducing dimensionless coordinates and time,

$$X \stackrel{\rm def}{=} \frac{x}{R}, \quad \tau \stackrel{\rm def}{=} t\sqrt{\frac{K\alpha_1 v}{\widetilde{h}}}, \tag{22}$$

we obtain the desired nonlinear differential second-order equation:

$$0 = \frac{d^2X}{d\tau^2} + \frac{dX}{d\tau}\sqrt{\frac{\widetilde{h}K}{v}}\left(1 + \frac{R\alpha_2}{\widetilde{h} + RX}\right) - (1 + kRX)\frac{\widetilde{h}}{R}\left(1 + \frac{R\alpha_2}{\widetilde{h} + RX}\right) + \frac{\widetilde{h}}{KvR}\frac{\rho_w - \rho_v}{\rho_w + \rho_v/2}g$$
$$+ \frac{3\widetilde{h}}{KvR}\frac{1}{\rho_w + \rho_v/2}\left\{-\frac{qE_0}{4\pi R^3}(1 + \lambda RX) - \varepsilon_0\frac{\varepsilon-1}{\varepsilon+2}\lambda E_0^2(1 + \lambda RX)\right\}. \tag{23}$$

4.4. Solution of the Equation of Motion

Equation (23) will be solved numerically using a standard computer program.

The solutions for a microdroplet disturbed from equilibrium exhibit an oscillatory character of motion (Fig. 7). The oscillation period is close to infrasonic. Note that signs of specifically infrasonic oscillations were found previously in variations in interdroplet distance [25]. Therefore, the vertical and horizontal oscillations of cluster microdroplets may be interrelated in some way.

The oscillatory character of solutions to Eq. (23) indicates that mechanical oscillations may be generated artificially using electrodynamic resonance or applying an intense acoustic wave directed along the x axis. The plots in Fig. 7 demonstrate an increase in the oscillation period of a microdroplet and its rise

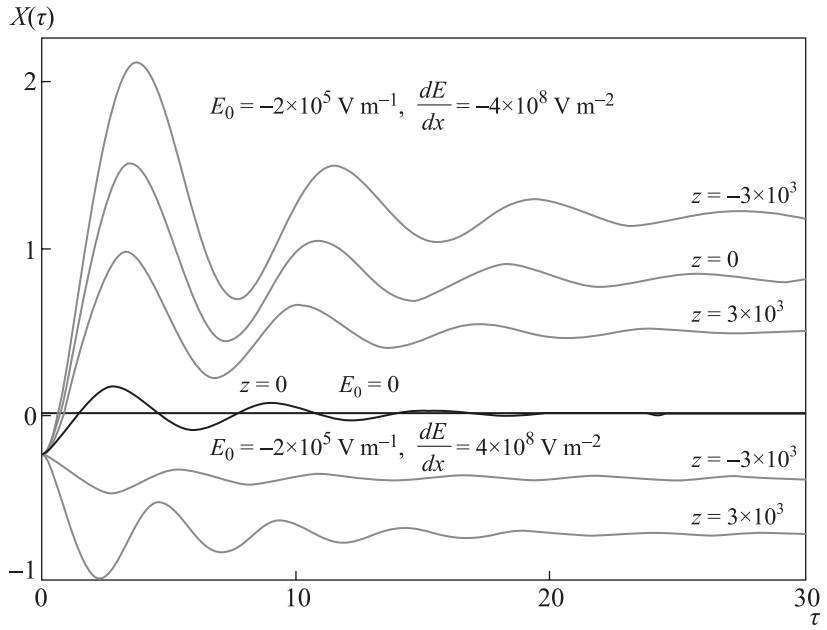

Fig. 7. Dependences of the microdroplet coordinate X on time τ at an initial deviation $X = -0.25$ in the absence and in the presence of field (black and gray curves, respectively).

to a new equilibrium height when an electric field is instantaneously switched on. In a strongly inhomogeneous field, where the DP force dominates over the EP force, the oscillatory motion and levitation height do not differ strongly for the cases of neutral and weakly charged microdroplets (the charge sign is of little importance). In this context, the model of electro-gravitational balance [4], which does not take into account the polarization in the low-electrode mode, should obviously be refined.

A direct comparison of the EP and DP forces shows that the maximin value of charge z (that is necessary to provide dominance of the DP force), expressed in terms of elementary charge e, does not exceed

$$z \leqslant \left| \frac{\wp_b}{eE_{\rm ex}} \frac{dE_{\rm ex}}{dx} \right| = \left| \frac{4\pi\varepsilon_0}{e} \frac{\varepsilon - 1}{\varepsilon + 2} R^3 \frac{dE}{dx} \right|. \qquad (24)$$

In the low-electrode mode (according to the scheme in Fig. 1), the field strength E may reach[1] 2×10^5 V m^{-1}, and the inhomogeneity $|dE/dx|$ is about 4×10^8 V m^{-2} ($\varphi_0 = 500$ V, $D = 1.5$ mm). Then, to make the DP force dominate over the EP force, the charge z should be no larger than 10^3 elementary charges. A droplet having this relatively low charge in region I (see Fig. 5) will be attracted to the upper electrode due to the DP force (as in Fig. 8) and to the lower electrode in region II. An analytical calculation shows the existence of this possibility; however, because of the limitations of the model considered in Subsec. 3.2, exact values of the interelectrode distance D and other parameters necessary for implementing this situation can be found only experimentally.

The logarithmic decrement Δ and frequency ω of microdroplet oscillations depend on different parameters (Figs. 8–10). According to numerical calculations, the oscillations of a neutral microdroplet are insensitive to the parameter $k < 0$ up to values on the order of 10^3 m^{-1}. With a further increase in k in modulus (which means a faster slowdown of the vapor-air flow with an increase in height), the frequency ω increases, while the decrement Δ (characterizing the energy loss) decreases (see Fig. 8), and the microdroplet hops on an air cushion. At the same time, a rise in the flow velocity v is accompanied by a decrease in ω and Δ (Fig. 9), because the resistance of the vapor-air medium enhances. The aforementioned regularities are retained qualitatively when an electric field is switched on (see Figs. 8 and 9); the only difference is that the Δ values (energy loss) are larger and the ω values are smaller in the presence of field.

The decrement and frequency depend weakly on amplitude (see Fig. 10). Therefore, the plots corresponding to instantaneous switching on a field (see Figs. 8 and 9) are representative, despite the jump of the equilibrium height, which leads to a significant jump of the oscillation amplitude (the initial deviation from zero in Fig. 7 is small in comparison with the microdroplet levitation height in electric field; therefore, in all cases, oscillations in field occur with an

[1] Breakdown in dry air occurs at a field strength of 3×10^6 V m^{-1} (for wet air, the breakdown threshold is somewhat higher).

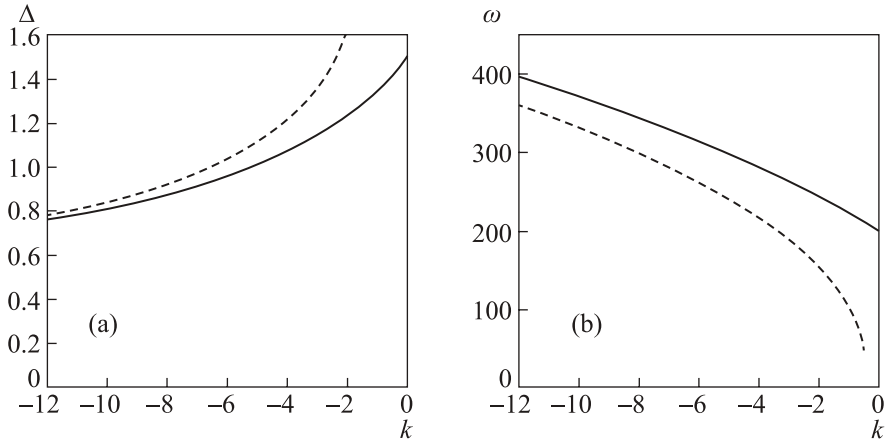

Fig. 8. Logarithmic decrement Δ (a) and damped natural frequency ω [s^{-1}] (b) of microdroplet oscillations in dependence on $k\times10^3$ [m^{-1}] ($z=0$). The solid and dashed curves correspond, respectively, to the absence of electric field and to instantaneously switched on electric field for the same droplet.

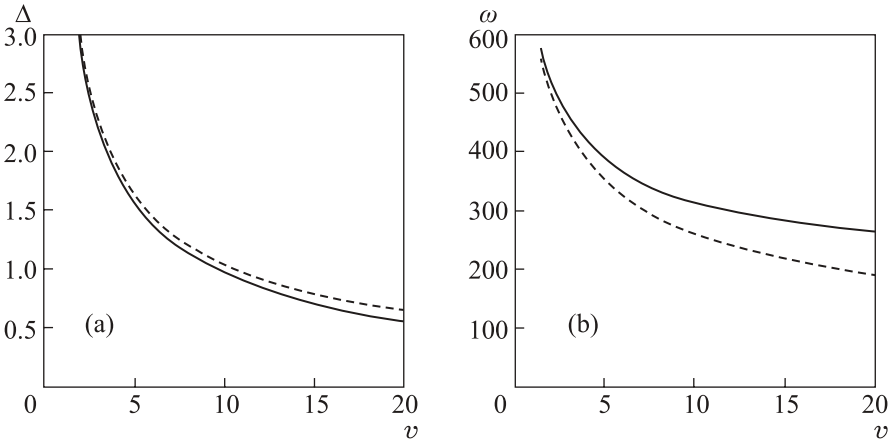

Fig. 9. Logarithmic decrement Δ (a) and damped natural frequency ω [s^{-1}] (b) of microdroplet oscillations in dependence on the flow velocity $v\times10^{-2}$ [$m\,s^{-1}$], $z=0$. The solid and dashed curves correspond, respectively, to the absence of electric field and to instantaneously switched on electric field, $E=-2\times10^{-5}$ V m^{-1}, $dE/dx=-4\times10^{8}$ V m^{-2}, for the same droplet.

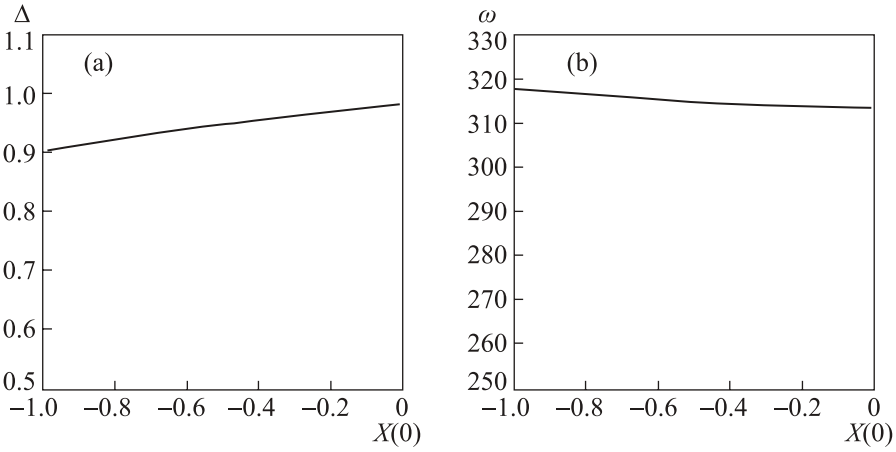

Fig. 10. Logarithmic decrement Δ (a) and damped natural frequency ω [s^{-1}] (b) in dependence on the initial deviation in the absence of electric field.

almost identical initial amplitude relative to the new equilibrium position).

Equation (23) clearly shows that electric field affects the microdroplet equilibrium position (which is almost completely determined by the free term in this equation). In a homogeneous field ($\lambda = 0$), the DP force is zero, and the droplet equilibrium position changes only due to the EP force.

The calculations revealed also a side effect: with all other parameters being fixed, there was a critical field in which the plot of microdroplet trajectory grew unlimitedly. This effect has a simple physical interpretation: the EK forces turned out to be sufficient to overcome the microdroplet gravity force). However, the analysis of the stability of solutions to (23), which must be performed in this case (in particular, via the Nyquist criterion [26]), is a nontrivial problem; this analysis has not been performed yet. In addition, in the absence of field, an instability occurs when k and α_2 in (23) are simultaneously zero, because stable equilibrium is impossible in this case.

Another interesting effect that can be investigated within model (23) is the artificial electrocoalescence with water surface. To implement it, one can use the high-electrode mode, in which region II is wide (see Fig. 3), or simply apply a potential φ_0 to the lower electrode. Electrocoalescence of microdroplets is easier to observe than their rise. Basically, this process has not been substantially analyzed for freely levitating microdroplets, although electrocoalescence has been studied for several decades [27–29]. In most cases, the electrocoalescence of droplets immersed in a fluid was considered [30, 31]. The process occurring on a substrate was studied in detail in [32].

Now it is clear that experiments on a droplet cluster make it possible to clarify to a great extent the precipitation processes occurring in thunderstorm clouds.

5. CONCLUSIONS

Thus, a theoretical model of mechanical motion of water microdroplets (forming a droplet cluster) in an external linear inhomogeneous electric field, with interdroplet interaction disregarded, was developed. The realistic field magnitude was calculated based on the proposed simplest experimental configuration of electrodes (see Fig. 1). The field distribution in this configuration is sensitive to the interelectrode distance (cf. Figs. 3 and 5). When the electrodes are located close to each other, the polarization forces are rather strong. In this context, the experimental and theoretical results reported in [4] can be significantly reinterpreted with allowance for the microdroplet polarization. According to Eq. (23), derived by us, the question of the presence, value, and sign of microdroplet charge can be solved experimentally by applying an ultimately homogeneous electric field, in which the contribution from the DP force is close to zero.

It was established theoretically that water microdroplets in a droplet cluster may occur vertical damping oscillations (see Fig. 7). Microdroplets are fairly sensitive to the presence of external electric field; therefore, as calculation examples showed, oscillations can be generated using an electrodynamic resonance or an acoustic wave. Then these oscillations can easily be observed at high amplitudes. It is difficult to perform experimental identification of oscillations on a low-sensitive equipment because of their high frequency and energy loss (see Figs. 8–10) and in view of the immanent mobility of the droplet cluster. The period and logarithmic decrement of oscillations are sensitive both to the vapor-air flow parameters and to the external field. The vertical-oscillation frequency and equilibrium levitation height depend on the value and sign of microdroplet charge in the cluster.

The external electric field may be so strong that the equilibrium height of microdroplets, depending on the electrokinetic force direction, will facilitate either their coalescence with the water layer or their arrival to the upper electrode. The same should occur when the field reaches the critical value, at which the solution to the equation of motion (23) loses stability. When the field is highly inhomogeneous, the critical strength may be lower than the breakdown strength for wet air; hence, this field can be implemented.

ACKNOWLEDGEMENTS

The author is grateful to Dr. S.N. Andreev for the preliminary simulation of electric fields in the KARAT software package.

The introductory review and calculations of electric fields in this study were supported by the Ministry of Education and Science of the Russian Federation (Project No. 3.8191.2017/БЧ). The derivation and solution of the equation of droplet motion were supported by the RFBR (Project 18-38-00232 mol_a).

REFERENCES

1. V.J. Schaefer, "Observation of an Early Morning Cup of Coffee," Am. Sci. **59**, 534 (1971).
2. A.A. Fedorets, "Droplet Cluster," JETP Lett. **79**, 372 (2004) [DOI: 10.1134/1.1772434].
3. A.A. Fedorets, "On the Mechanism of Noncoalescence in a Droplet Cluster," JETP Lett. **81**, 437 (2005) [DOI: 10.1134/1.1984025].

4. A.V. Shavlov, V.A. Dzhumandzhi, and S.N. Romanyuk, "Electrical Properties of Water Drops inside the Dropwise Cluster," Phys. Lett. A. **376**, 39 (2011) [DOI: 10.1016/j.physleta.2011.10.032].
5. A.A. Fedorets, L.A. Dombrovsky, and D.N. Medvedev, "Effect of Infrared Irradiation on the Suppression of the Condensation Growth of Water Droplets in a Levitating Droplet Cluster," JETP Lett. **102**, 452 (2015) [DOI: 10.1134/S0021364015190042].
6. L.A. Dombrovsky, A.A. Fedorets, and D.N. Medvedev, "The Use of Infrared Irradiation to Stabilize Levitating Clusters of Water Droplets," Infrar. Phys. Technol. **75**, 124 (2016) [DOI: 10.1016/j.infrared.2015.12.020].
7. V.A. Dzhumandzhi, Abstract of the Thesis "The Physical Properties of an Ordered Aqueous Aerosol—a Droplet Cluster" (Tyumen, 2013), p. 8 [in Russian].
8. A.V. Fillipov, A.F. Pal', and A.N. Starostin, "Electrostatic Interaction of Two Charged Macroparticles in an Equilibrium Plasma," JETP. **121**(5), 909 (2015) [DOI: 10.1134/S1063776115110035].
9. V.A. Saranin, "Possibility of the Levitation of Droplets in the Atmosphere When They Are Charged by Induction in an Electric Field under Nonuniform Evaporation Conditions," Tech. Phys. **43**(2), 145 (1998) [DOI: 10.1134/1.1258958].
10. A.V. Shavlov, V.A. Dzhumandzhi, and A.A. Yakovenko, "Charge Separation at the Evaporation (Condensation) Front of Water and Ice. Charging of Spherical Droplets," Tech. Phys. **63**(4), 482 (2018) [DOI: 10.21883/JTF.2018.04.45716.2463].
11. M.A. Leontovich, *Introduction to Thermodynamics. Statistical Physics* (Nauka, Moscow, 1983) [in Russian].
12. L. Ying, S.S. White, A. Bruckbauer, L. Meadows, Yu.E. Korchev, and D. Klenerman, "Frequency and Voltage Dependence of the Dielectrophoretic Trapping of Short Lengths of DNA and dCTP in a Nanopipette," Biophys. J. **86**, 1018 (2004) [DOI: 10.1016/S0006-3495(04)74177-6].
13. L.D. Landau and E.M. Lifshitz, *Course of Theoretical Physics*, Vol. 8: *Electrodynamics of Continuous Media*, 2nd ed. (Pergamon Press, Oxford, 1984).
14. S.N. Manida, *Physics. Solution of Tasks of Elevated Complexity: Based on the Materials of the City Schoolchildren Olympiads: Tutorial* (St. Petersburg State University, St. Petersburg, 2004), pp. 10, 398 [in Russian].
15. A.A. Fedorets, I.V. Marchuk, and O.A. Kabov, "Role of Vapor Flow in the Mechanism of Levitation of a Droplet-Cluster Dissipative Structure," Tech. Phys. Lett. **37**(2), 116 (2011) [DOI: 10.1134/S1063785011020064].
16. A.A. Fedorets, M. Frenkel, E. Shulzinger, and L.A. Dombrovsky, "Self-Assembled Levitating Clusters of Water Droplets: Pattern-Formation and Stability," Sci. Rep. **7**(1), 1888 (2017) [DOI: 10.1038/s41598-017-02166-5].
17. L.D. Landau and E.M. Lifshitz, *Fluid Mechanics* (Pergamon Press, Oxford, 1987).
18. A.A. Fedorets, "Mechanism of Stabilization of Location of a Droplet Cluster above the Liquid-Gas Interface," Tech. Phys. Lett. **38**(11), 988 (2012) [DOI: 10.1134/S1063785012110077].
19. A. Ogbi, L. Nicolas, R. Perrussel, and D. Voyer, "Calculation of DEP Force on Spherical Particle in Non-Uniform Electric Fields," NUMELEC (July 2012, Marseille, France), p. 180 (2012) [www.hal.archives-ouvertes.fr/hal-00714500].
20. M. Esseling, *Photorefractive Optoelectronic Tweezers and Their Applications* (Springer, 2015), Sec. 2, p. 13 [DOI: 10.1007/978-3-319-09318-5].
21. V.A. Saranin, "On the Interaction of Two Electrically Charged Conducting Balls," Phys.-Usp. **42**, 385 (1999).
22. E.A. Shcherba, A.I. Grigor'ev, and V.A. Koromyslov, "On Interaction of Two Closely Spaced Charged Conducting Spheres," Tech. Phys. **47**(1), 13 (2002) [DOI: 10.1134/1.1435884].
23. J. Lekner, "Electrostatics of Two Charged Conducting Spheres," Proc. Roy. Soc. A. **468**, 2829 (2012) [DOI: 10.1098/rspa.2012.0133].
24. E.L. Tarunin, "The Dinamics of Charged Conductiong Balls Near the Inversion of the Force of Electrostatic Repulsion," Bull. Perm Univ. **1**(36), 41 (2017) [www.vestnik.psu.ru/select_box.php?num=1&year=2017] [in Russian].
25. A.V. Shavlov, V.A. Dzhumandzhi, and S.N. Romanyuk, "Sound Oscillation of Dropwise Cluster," Phys. Lett. A. **375**, 2049 (2012) [DOI: 10.1016/j.physleta.2012.05.012].
26. V.A. Besekerskij and E.P. Popov, *Theory of Automatic Control Systems* (Nauka, St. Petersburg, 1975) [in Russian].
27. G.G. Goyer, J.E. McDonald, F. Baer, and R.R. Braham, Jr., "Effects of Electric Fields on Water-Droplet Coalescence," J. Meteorology. **17**, 442 (1960) [DOI: 10.1175/1520-0469(1960)017<0442:EOEFOW>2.0.CO;2].
28. G. Freier, "The Coalescence of Water Drops in an Electric Field," J. Geophys. Res. **65**, 1979 (1960) [DOI: 10.1029/JZ065i012p03979].
29. C.H. Hendricks and R.G. Semonin, Investigation of Water Droplet Coalescence (1963) [www.isws.illinois.edu/pubdoc/CR/ISWSCR-48.pdf].
30. M. Mohammadi, Sh. Shahhosseini, and M. Bayat, "Numerical Study of the Collision and Coalescence of Water Droplets in an Electric Field," Chem. Eng. Technol. **37**, 27 (2014) [DOI: 10.1002/ceat.201200479].
31. M. Brik, R. Ruscassie, and A. Saboni, "Droplet Deformation and Coalescence under Uniform Electric Field," J. Chem. Tech. Metal. **51**, 647 (2016) [www.dl.uctm.edu/journal/node/78].
32. J. Ndoumbe, A. Beroual, and A.M. Imano, "Simulation and Analysis of Coalescence of Water Droplets on Composite Insulating Surface under DC Electric Field," IEEE Trans. Diel. Electr. Insul. **22**, 2669 (2015) [DOI: 10.1109/TDEI.2015.004820].

APPENDIX

Proceeding from Gauss's law, one can show that the potential at a point located at height $h \geqslant 0$ above a thin uniformly charged disk of radius a with a surface charge density $\sigma_{\rm d}$ at a distance s from its axis, has the form

$$\varphi_{\rm disk}(h,s,\sigma_{\rm d}) = \frac{\sigma_{\rm d}}{4\pi\varepsilon_0}\left\{2\pi\left[\sqrt{(a-s)^2+h^2}-h\right]+2\int\limits_{a-s}^{a+s}\frac{\rho}{\sqrt{\rho^2+h^2}}\arccos\left(\frac{\rho^2-a^2+s^2}{2s\rho}\right)d\rho\right\}. \quad (A.1)$$

The strength components that are parallel and perpendicular to the disk axis can be written as ($h \geqslant 0$)

$$E_{\rm disk\|}(h,s,\sigma_{\rm d}) = \frac{\sigma_{\rm d}}{4\pi\varepsilon_0}\left\{2\pi\left[1-\frac{h}{\sqrt{(a-s)^2+h^2}}\right]+2\int\limits_{a-s}^{a+s}\frac{rh}{(r^2+h^2)^{3/2}}\arccos\left(\frac{r^2-a^2+s^2}{2rs}\right)dr\right\},$$

$$E_{\rm disk\perp}(h,s,\sigma_{\rm d}) = \frac{\sigma_{\rm d}}{4\pi\varepsilon_0}\,2\int\limits_{a-s}^{a+s}\frac{r^2}{(r^2+h^2)^{3/2}}\arccos\left(\frac{r^2-a^2+s^2}{2rs}\right)dr. \quad (A.2)$$

In particular, on the disk axis,

$$\varphi_{\rm disk}(h,0,\sigma_{\rm d}) = \frac{\sigma_{\rm d}}{2\varepsilon_0}\left[\sqrt{a^2+h^2}-h\right], \quad (A.3)$$

$$E_{\rm disk\|}(h,0,\sigma_{\rm d}) = \frac{\sigma_{\rm d}}{2\varepsilon_0}\left[1-\frac{h}{\sqrt{(a-s)^2+h^2}}\right], \quad E_{\rm disk\perp}(h,0,\sigma_{\rm d}) \equiv 0.$$

Obviously, the quantities $\varphi_{\rm b}$, $E_{\rm b\|}$, and $E_{\rm b\perp}$, formed by the lower disk electrode in the system described in Sec. 3, are, respectively, the quantities $\varphi_{\rm disk}$, $E_{\rm disk\|}$, and $E_{\rm disk\perp}$ in Eqs. (A3).

The field at a point located at a distance r from the end face of a uniformly charged cylinder of length $2L$ and radius $a_{\rm c} = d/2$, with a surface charge density $\sigma_{\rm c}$, and a distance s from the cylinder axis is the sum of the fields from the lateral surface and end faces of this cylinder:

$$\varphi_{\rm cyl}(r,s,\sigma_{\rm c}) = \frac{a_{\rm c}\sigma_{\rm c}}{2\pi\varepsilon_0}\int\limits_0^{2L}\int\limits_0^{\pi}\frac{1}{\sqrt{(r+z)^2+a_{\rm c}^2+s^2-2a_{\rm c}s\cos\alpha}}\,d\alpha\,dz+\varphi_{\rm disk}(r,s,\sigma_{\rm c})+\varphi_{\rm disk}(r+2L,s,\sigma_{\rm c}),$$

$$E_{\rm cyl}(r,s,\sigma_{\rm c}) = -\mathrm{grad}\,\varphi_{\rm disk}(r,s,\sigma_{\rm c})\ (\sigma \equiv \mathrm{const}). \quad (A.4)$$

In particular, on the cylinder axis ($s = 0$),

$$\varphi_{\rm cyl}(r,0,\sigma_{\rm c}) = \frac{\sigma_{\rm c}}{2\varepsilon_0}\left\{a_{\rm c}\left[\mathrm{arsinh}\left(\frac{r+2L}{a_{\rm c}}\right)-\mathrm{arsinh}\left(\frac{r}{a_{\rm c}}\right)\right]+\sqrt{a_{\rm c}^2+r^2}-r+\sqrt{a_{\rm c}^2+(r+2L)^2}-r-2L\right\},$$

$$E_{\rm cyl\|}(r,\sigma_{\rm c}) = \frac{\sigma_{\rm c}}{2\varepsilon_0}\left[\frac{a_{\rm c}}{\sqrt{a_{\rm c}^2+r^2}}-\frac{a_{\rm c}}{\sqrt{a_{\rm c}^2+(r+2L)^2}}+1-\frac{r}{\sqrt{a_{\rm c}^2+r^2}}+1-\frac{r+2L}{\sqrt{a_{\rm c}^2+(r+2L)^2}}\right], \quad (A.5)$$

$$E_{\rm cyl\perp}(h,s,\sigma_{\rm c}) \equiv 0.$$

Here, it is also obvious that the quantities $\varphi_{\rm u}$, $E_{\rm u\|}$, and $E_{\rm u\perp}$, which are formed by the upper wire electrode in the system considered in Sec. 3, are, respectively, the quantities $\varphi_{\rm cyl}$, $E_{\rm cyl\|}$, and $E_{\rm cyl\perp}$.

The expression for the surface charge density on a disk was presented in Subsec. 3.1 by an example of $\sigma_{\text{b|ind}}$ (see (1)). The surface charge density on a uniformly charged cylinder is proportional to the potential φ_0 applied to it,

$$\sigma_{\text{cyl}} = \frac{\varphi_0 C_u}{2\pi a_{\text{c}}(a_{\text{c}} + 2L)} = \frac{\varphi_0 C_u}{\pi d(d/2 + 2L)}. \quad \text{(A.6)}$$

To calculate these surface charge densities, it is necessary to know the electric capacitances of the upper and lower electrodes, which can be approximated by, respectively, elongated and flattened ellipsoids. In our designations, their capacitances can be written as [13]

$$C_u = 4\pi\varepsilon_0 \frac{\sqrt{L^2 - (d/2)^2}}{\operatorname{arcosh}(2L/d)} \approx \frac{4\pi\varepsilon_0 L}{\operatorname{arcosh}(2L/d)}, \quad \text{(A.7)}$$

$$C_b = 4\pi\varepsilon_0 \frac{\sqrt{a^2 - (\delta_{\text{ox}}/2)^2}}{\arccos(\delta_{\text{ox}}/2a)} \approx 8\varepsilon_0 a.$$